Large-scale silicon quantum photonics implementing arbitrary two-qubit processing

Xiaogang Qiang,[1,3,4] Xiaoqi Zhou,[2,1,*] Jianwei Wang,[1] Callum M. Wilkes,[1] Thomas Loke,[5] Sean O'Gara,[1] Laurent Kling,[1] Graham D. Marshall,[1] Raffaele Santagati,[1] Timothy C. Ralph,[6] Jingbo B. Wang,[5] Jeremy L. O'Brien,[1] Mark G. Thompson,[1] and Jonathan C. F. Matthews[1,†]

[1] *Quantum Engineering Technology Labs, H. H. Wills Physics Laboratory and Department of Electrical & Electronic Engineering, University of Bristol, BS8 1FD,UK.*
[2] *State Key Laboratory of Optoelectronic Materials and Technologies and School of Physics, Sun Yat-sen University, Guangzhou 510275, China*
[3] *State Key Laboratory of High Performance Computing and School of Computer Science, NUDT, Changsha 410073, China*
[4] *National Innovation Institute of Defense Technology, AMS, Beijing 100071, China*
[5] *School of Physics, The University of Western Australia, Crawley WA 6009, Australia*
[6] *Centre for Quantum Computation and Communication Technology, Department of Mathematical and Physics, The University of Queensland, St. Lucia, Queensland 4072, Australia*

(Dated: April 15, 2018)

Integrated optics is an engineering solution proposed for exquisite control of photonic quantum information. Here we use silicon photonics and the linear combination of quantum operators scheme to realise a fully programmable two-qubit quantum processor, which enables universal two-qubit quantum information processing in optics for the first time. The device is fabricated with readily available CMOS based processing and comprises four nonlinear photon-sources, four filters, eighty-two beam splitters and fifty-eight individually addressable phase shifters. To demonstrate performance, we programmed the device to implement ninety-eight various two-qubit unitary operations (with average quantum process fidelity of 93.2±4.5%), a two-qubit quantum approximate optimization algorithm and efficient simulation of Szegedy directed quantum walks. This fosters further use of the linear combination architecture with silicon photonics for future photonic quantum processors.

The range and quality of control that a device has over quantum physics determines the extent of quantum information processing (QIP) tasks that it can perform. One device capable of performing any given QIP task is an ultimate goal[1] and silicon quantum photonics[2] has attractive traits to achieve this: photonic qubits are robust to environmental noise[3], single qubit operations can be performed with high precision[4], a high density of reconfigurable components have been used to manipulate coherent light[5,6] and established fabrication processes are CMOS compatible. However, quantum control needs to include entangling operations to be relevant to QIP — this is recognised as one of the most challenging tasks for photonics because of the extra resources required for each entangling step[3,7]. Here, we demonstrate a programmable silicon photonics chip that generates two photonic qubits, on which it then performs arbitrary two-qubit untiary operations, including arbitrary entangling operations. This is achieved by using silicon photonics to reach the complexity required to implement an iteration of the linear combination of unitaries architecture[8,9] that we have adapted to realise universal two-qubit processing. The device's performance shows that the design and fabrication techniques used in its implementation work well with the linear combination architecture and can be used to realise larger and more powerful photonic quantum processors.

Miniaturisation of quantum-photonic experiments into chip-scale waveguide circuits started[10] from the need to realise many-mode devices with inherent sub-wavelength stability for generalised quantum-interference experiments, such as multi-photon quantum walks[11] and boson sampling[12–14]. Universal six-mode linear optics implemented with a silica waveguide chip (coupled to free-space photon sources and fibre-coupled detectors) demonstrated the principle that single photonic devices can be configured to perform any given linear optics task[15]. Silicon waveguides promise even greater capability for large-scale photonic processing, because of their third order nonlinearity that enables photon pair generation within integrated structures[16], their capacity for integration with single photon detectors[17] and their component density can be more than three orders of magnitude higher than silica[2].

Programmable quantum processors have been reported with up to five trapped-ion qubits[18], eleven NMR qubits[19] and tens of superconducting qubits[20]. However, for photons, up to two sequential two-qubit entangling operations implemented with free-space optics[21,22] and silicon quantum photonics[23,24] is the state of the art in qubit control. But the degree of control and utility of these photonic demonstrators is limited intrinsically because arbitrary two-qubit processing requires the equivalent of three consecutive entangling gates in the circuit model of quantum computing, as demonstrated experimentally in 2010 with ion-trap quantum processing[25]. Effective QIP with three sequential entangling operations is beyond the level of complexity that can be practically constructed and maintained with free-space quantum optics or a hybrid of free-space nonlinear optics and integrated linear optics[15].

Our scheme realizes arbitrary two-qubit unitary operation via a linear combination of four easy-to-implement unitaries — each being a tensor product

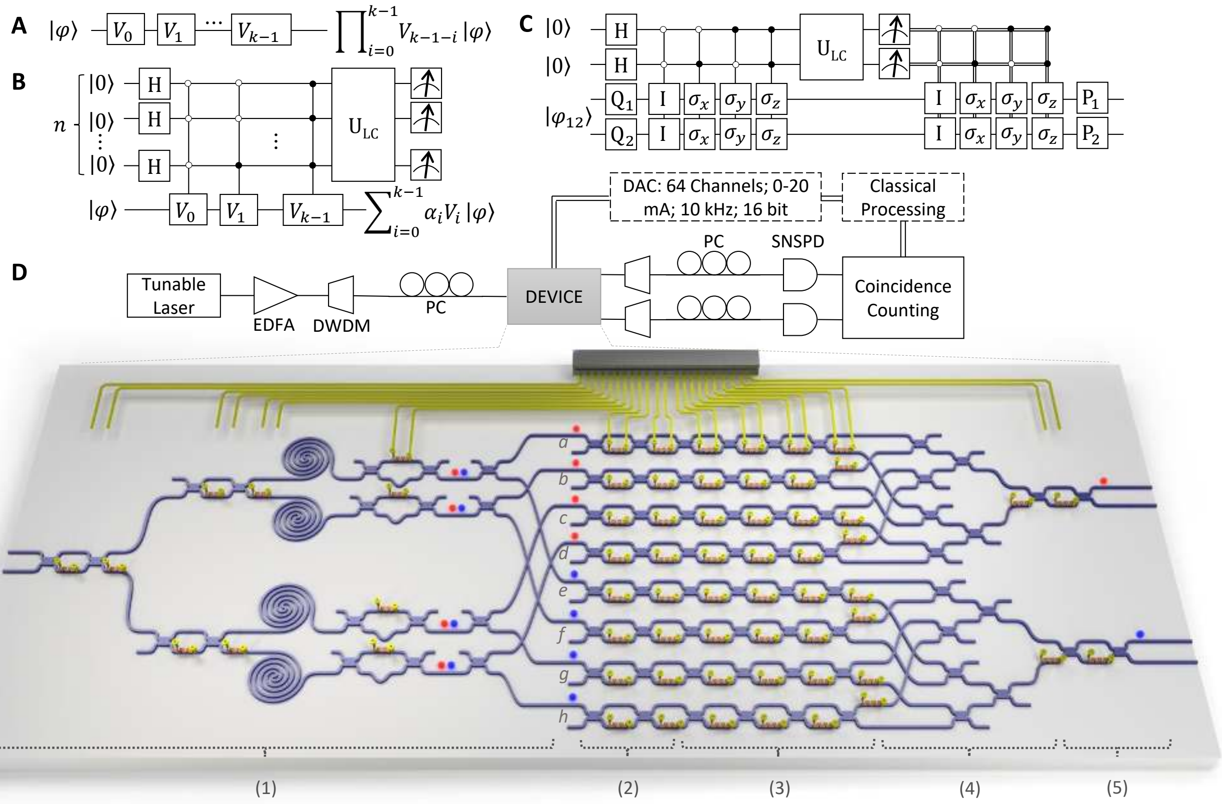

FIG. 1: **Quantum information processing circuits and a schematic of the experimental setup.** (A) The conventional quantum circuit model of QIP, that is a multiplication of quantum logic gates in series. (B) Probabilistic linear-combination of quantum gates. The operation $\sum_{i=0}^{k-1}\alpha_i V_i$ is implemented when all n control qubits are measured to be 0. U_{LC} is a unitary operation with first row in its matrix representation given as $\{\alpha_0, \alpha_1, \cdots, \alpha_{n-1}\}$ where $\sum_{i=0}^{k-1}|\alpha_i|^2 = 1$, $k = 2^n$ and the success probability is $1/k$. Other rows are chosen accordingly to make U_{LC} unitary. (C) Deterministic linear-combination circuit for universal two-qubit unitary operation. For a $U \in \mathrm{SU}(4)$ being decomposed as Equation (1), U_{LC} is defined as $[\alpha_0, \alpha_1, \alpha_2, \alpha_3; \alpha_1, \alpha_0, -\alpha_3, -\alpha_2; \alpha_2, -\alpha_3, \alpha_0, -\alpha_1; \alpha_3, -\alpha_2, -\alpha_1, \alpha_0]$. $|\varphi_{12}\rangle$ is an arbitrary two-qubit state. The required two auxiliary control qubits can also be replaced by a ququart (four-level system) and then U_{LC} is a single-ququart operation. (D) Schematic of our device and external setup. A tunable continuous wave laser is amplified with an optical fibre amplifier (EDFA), spectrally filtered by a dense wavelength-division multiplexing (DWDM) module and launched into the device through a V-groove fibre array (VGA). Photons emerging from the device are collected by the same VGA and two DWDMs are used to separate the signal (red) and idler (blue) photons. Photons are detected by two fibre-coupled superconducting nanowire single-photon detectors (SNSPD). The polarisations of input/output photons are optimised by in-line polarization controllers (PC). Coincidence counting logic records the two-photon coincidence events. Phase shifters on the device are configured through a digital-to-analog converter (DAC), controlled from a computer. The device includes five functional parts: (1) generating ququart-entanglement; (2) preparing initial single-qubit states; (3) implementing single-qubit operations; (4) realizing linear-combination; (5) changing the measurement basis. Part (1), (3) and (4), as a whole, are used to implement a given SU(4) operation, where part (1) encodes the linear-combination coefficients, part (3) implements linear terms A_i and B_i and part (4) realizes the linear combination of terms $A_i \otimes B_i$ together with post-selection. Part (2) prepares arbitrary separable two-qubit states $|\varphi_{ini}\rangle$ $(= |\varphi_1\rangle \otimes |\varphi_2\rangle)$ as the input, which is independent of the implemented gate. Part (5) rotates the output state so that it can be measured at desired basis.

of two single-qubit unitaries. The presented chip constructs and exploits high-dimensional entanglement in order to implement the equivalent capability of three sequential entangling gates in the circuit model whilst using only two photons. It performs universal two-qubit processing with high fidelity whilst all thermal phase shifters in the device are simultaneously active and it possesses inherent phase stability of the optical paths and waveguide interferometric structures. The chip is also repeatable under continuous operation and it can be reprogrammed at kilohertz rate. We demonstrate the chip's performance by performing process tomography on 98 implemented two-qubit quantum logic gates, by realising the quantum approximate optimization algorithm (QAOA)[26,27] applied to three example constraint satisfaction problems, and by simulating Szegedy quantum walks (SQW)[28,29] over an example two-node weighted graph. All together, the results presented required 98480 experiment configurations.

1. Linear combination of unitaries on a chip for QIP. The conventional quantum circuit model for QIP is a sequence of quantum gates (Fig. 1(A)). The linear combination of unitary operations is an alternative approach (Fig. 1(B)) that is central to various QIP tasks[8,30–34]. A universal two-qubit unitary $U \in \mathrm{SU}(4)$ can be implemented by the four-operator linear combination[35]

$$U = \sum_{i=0}^{3} \alpha_i \left(P_1 \sigma_i Q_1\right) \otimes \left(P_2 \sigma_i Q_2\right), \quad (1)$$

where P and Q are single-qubit gates, σ_i are identity and Pauli gates (I, σ_x, σ_y, σ_z) and α_i are complex coefficients satisfying $\sum_{i=0}^{3} |\alpha_i|^2 = 1$. This linear combination can immediately be implemented through two-qubit version of the n-qubit circuit shown in Fig. 1(B), with an intrinsic success probability of 1/4. However, we also note that a deterministic implementation of the linear-combination of U can in principle be achieved with extra classical controlled gates[35], as shown in Fig. 1(C). In the presented chip, the linear decomposition of U is implemented probabilistically by expanding the dimension of qubits into qudits and using pre-entanglement between qudit systems that can be generated from parametric photon pair generation[8,23]. This Hilbert-space-expansion approach implements arbitrary two-qubit unitaries using resources of only a two-photon entangled-ququart state and multimode interferometry[35], that is inherently stable on our chip.

Fig. 1(D) illustrates the schematic of our silicon photonic chip operated with external electrical control, laser input and fibre coupled superconducting detectors. The 7.1 mm × 1.9 mm chip consists of four spiral-waveguide spontaneous four-wave mixing (SFWM) photon-pair sources[36], four laser pump rejection filters, eighty-two multi-mode interferometer (MMI) beam splitters and fifty-eight simultaneously running thermo-optic phase shifters[36]. Within the device, the four SFWM sources are used to create possible (signal-idler) photon pairs when pumped with a laser that is launched into the chip and split across the four sources according to complex coefficients α_i. The spatially bunched photon pairs are coherently generated in either one of the four sources. Post-selecting when signal and idler photons exit at the top two output modes (qubit 1) and the bottom two (qubit 2) respectively, yields a path-entangled ququart state $|\Phi\rangle$ as

$$\alpha_0 |1\rangle_a |1\rangle_e + \alpha_1 |1\rangle_b |1\rangle_f + \alpha_2 |1\rangle_c |1\rangle_g + \alpha_3 |1\rangle_d |1\rangle_h \quad (2)$$

at the end of stage (1) marked on the device shown in Fig. 1(D), with intrinsic success probability of 1/4. $|1\rangle_j$ represents the Fock state in spatial modes labeled by $j = a, b, c, d, e, f, g, h$.

Spatial modes a-h are each extended into two modes to form path-encoded single-qubit states $|\varphi_1\rangle$ or $|\varphi_2\rangle$ with arbitrary amplitude and phase controlled with Mach-Zehnder Interferometers (MZI) and an extra phase shifter. Single-qubit operations A_i ($=P_1\sigma_i Q_1$) and B_i ($=P_2\sigma_i Q_2$) are applied using MZIs and phase shifters to $|\varphi_1\rangle$ and $|\varphi_2\rangle$ respectively, evolving $|\Phi\rangle$ into

$$\sum_{i=0}^{3} \alpha_i A_i |\varphi_1\rangle_{u^i} B_i |\varphi_2\rangle_{v^i}, \quad (3)$$

where $u^i \in \{a, b, c, d\}$ and $v^i \in \{e, f, g, h\}$. Next, the qubits a, b, c, d are combined into one final-stage qubit, and the qubits e, f, g, h into the remaining final-stage qubit, as shown in stage (4) of Fig. 1(D) with intrinsic success probability 1/16. This removes path information of the signal (idler) photon and thus we obtain the final evolved two-photon state as

$$\left(\sum_{i=0}^{3} \alpha_i A_i \otimes B_i\right) |\varphi_{ini}\rangle \quad (4)$$

where $|\varphi_{ini}\rangle$ ($= |\varphi_1\rangle \otimes |\varphi_2\rangle$) is an arbitrary separable two-qubit state. Once photons are generated, the overall intrinsic success probability of our design is 1/64, which is higher than the two main schemes considered for universal linear optical quantum computation[35]: the Knill-Laflamme-Milburn (KLM) scheme[7] and linear optical measurement-based quantum computation (MBQC)[37]. The success probability of this optical implementation could be further increased to 1/4 if we were to separate signal and idler photons with certainty and use also an advanced linear-combination circuit that utilizes the unused optical ports in our current chip design[35].

2. Realising individual quantum gates. The linear-combination scheme can simplify implementation of families of two-qubit gates. For example, an arbitrary two-qubit controlled-unitary gate CU can be implemented as the linear combination of two terms:

$$\mathrm{CU} = \frac{1}{\sqrt{2}} \begin{pmatrix} 1 & 0 \\ 0 & i \end{pmatrix} \otimes \frac{I - iU}{\sqrt{2}} + \frac{1}{\sqrt{2}} \begin{pmatrix} 1 & 0 \\ 0 & -i \end{pmatrix} \otimes \frac{I + iU}{\sqrt{2}}, \quad (5)$$

and SWAP gate can be implemented by a linear combination of only identity and Pauli gates:

$$\mathrm{SWAP} = \frac{1}{2} \left(I \otimes I + \sigma_x \otimes \sigma_x + \sigma_y \otimes \sigma_y + \sigma_z \otimes \sigma_z\right). \quad (6)$$

To show the reconfigurability and performance of our chip, we implemented 98 different two-qubit quantum logic gates, for which we performed on-chip full quantum process tomography and reconstructed the process matrix using the maximum likelihood estimation technique for each gate[35]. A histogram of measured process fidelities for these 98 gates is shown in Fig. 2(A), with a mean statistical fidelity of 93.15±4.53%. The implemented gates include many common instances—as shown in Fig. 2(B, C)—achieving high fidelities, such as CNOT with 98.85±0.06% and SWAP with 95.33±0.24%. Our device also allows implementation of non-unitary quantum operations. The entanglement filter (EF)[8,38] and the entanglement splitter (ES)[8] can be implemented by

$$\mathrm{EF} = \left(I \otimes I + \sigma_z \otimes \sigma_z\right)/\sqrt{2} \quad (7)$$

$$\mathrm{ES} = \left(I \otimes I - \sigma_z \otimes \sigma_z\right)/\sqrt{2} \quad (8)$$

The results are shown in Fig. 2(D) and (E) in the form of logical basis truth tables, with the classical fidelities of 95.31±0.45% and 97.69±0.31% respectively. A further discussion about the experimental fidelities is presented in the Supplementary Information.

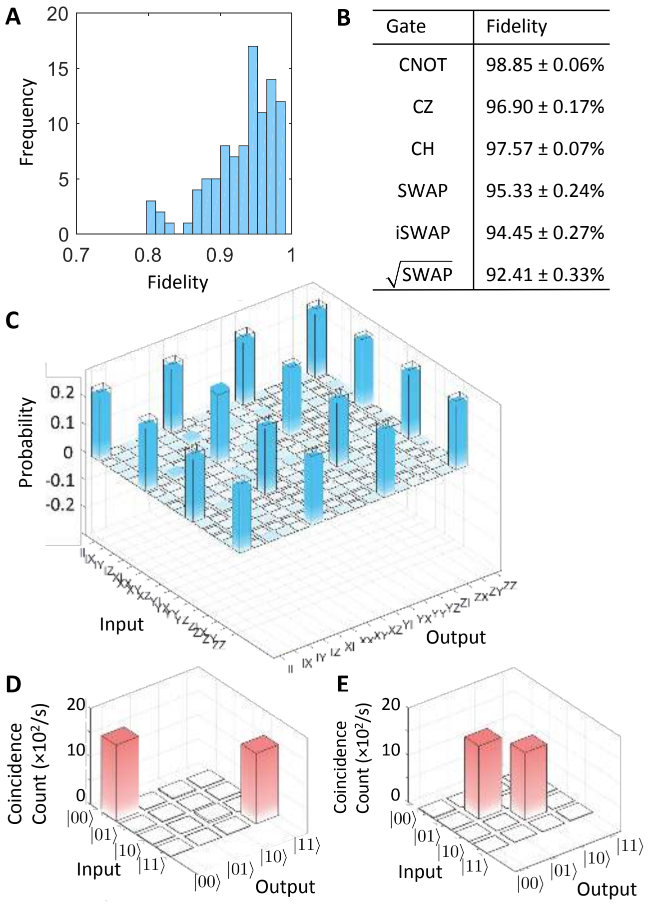

Gate	Fidelity
CNOT	98.85 ± 0.06%
CZ	96.90 ± 0.17%
CH	97.57 ± 0.07%
SWAP	95.33 ± 0.24%
iSWAP	94.45 ± 0.27%
$\sqrt{\text{SWAP}}$	92.41 ± 0.33%

FIG. 2: **Experimental realisation of arbitrary 2-qubit gates.** (A) A histogram of measured process fidelities for 98 two-qubit quantum gates ($\bar{F} = 93.15 \pm 4.53\%$). (B) Measured process fidelities for example two-qubit gates: C-NOT, C-Z, C-H, SWAP, iSWAP, $\sqrt{\text{SWAP}}$. The errors are estimated by adding random noise to the raw data and performing many reconstructions. (C) The real part of experimentally determined process matrices of SWAP, with ideal theoretical values overlaid. (D, E) Logical basis truth tables for entanglement filter (D) and entanglement splitter (E).

3. Implementing a two-qubit Quantum Approximate Optimization Algorithm for Constraint Satisfaction Problems. The quantum approximate optimization algorithm (QAOA) was proposed for finding approximate solutions to combinatorial search problems such as constraint satisfaction problems (CSPs)[26,27]. It is a promising candidate to run on primitive quantum computers because of its possible use for optimization and its conjectured potential as a route to establishing quantum supremacy[39]. A general CSP is specified by n bits and a collection of m constraints—each of which involves

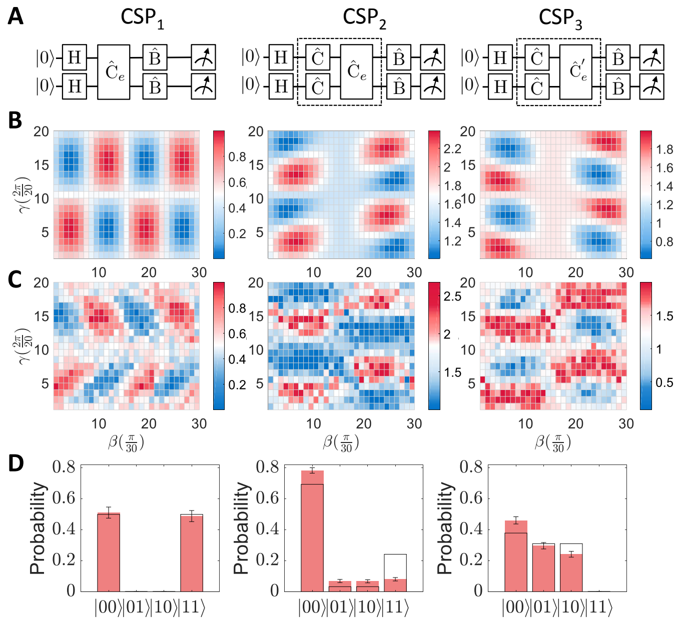

FIG. 3: **Experimental realisation of a two-qubit quantum approximate optimisation algorithm.** Panels arranged into three columns, corresponding to three example CSPs, labeled 1-3. (A) Quantum circuits of QAOA for each CSP. (B) Theoretical and (C) experimentally determined values of $\langle\gamma, \beta|C|\gamma, \beta\rangle$ over the grid of $[\gamma, \beta] \in [0, 2\pi] \times [0, \pi]$ for CSP_1, CSP_2 and CSP_3, with step size $\delta_\gamma = \frac{2\pi}{20}, \delta_\beta = \frac{\pi}{30}$, for finding the optimized $|\gamma, \beta\rangle$ states. (D) Experimental measurement results of the optimized $|\gamma, \beta\rangle$ states, outputting the searched target string z for each CSP 1-3. The s.d. of each individual probability is calculated by propagating error assuming Poissonian statistics.

a small subset of the bits. For a CSP, QAOA outputs a binary string z which (approximately) maximizes the number of satisfied constraints, i.e., $C(z) = \sum_{l=1}^m C_l(z)$ where $C_l(z) = 1$ if z satisfies the l-th constraint, otherwise 0 — this is the goal of CSP.

The QAOA process can be summarised as follows. Suppose two operators C and B are defined as

$$C\,|z\rangle := C(z)\,|z\rangle\,,\ B := \sum_{i=1}^n \sigma_x^{(i)} \tag{9}$$

where $\sigma_x^{(i)}$ represents σ_x acting on the i-th qubit, and a quantum state $|\vec{\gamma}, \vec{\beta}\rangle$ is defined as

$$|\vec{\gamma}, \vec{\beta}\rangle = e^{-i\beta_p B} e^{-i\gamma_p C} \cdots e^{-i\beta_1 B} e^{-i\gamma_1 C} H^{\otimes n}\,|0\rangle^{\otimes n} \tag{10}$$

where $\vec{\gamma} := (\gamma_1, \cdots, \gamma_p) \in [0, 2\pi]^p$ and $\vec{\beta} := (\beta_1, \cdots, \beta_p) \in [0, \pi]^p$. QAOA seeks the target string z by searching the $\vec{\gamma}$ and $\vec{\beta}$ that maximize $\langle\vec{\gamma}, \vec{\beta}|C|\vec{\gamma}, \vec{\beta}\rangle$ and then the corresponding state $|\vec{\gamma}, \vec{\beta}\rangle$ in the computational basis encodes the solution. For a given $\vec{\gamma}$ and $\vec{\beta}$, $\langle\vec{\gamma}, \vec{\beta}|C|\vec{\gamma}, \vec{\beta}\rangle$ can be evaluated through a quantum computer, which can further be used as a subroutine in an enveloping classical algorithm—for example, run the quantum computer with angles $(\vec{\gamma}, \vec{\beta})$ from a fine grid on the

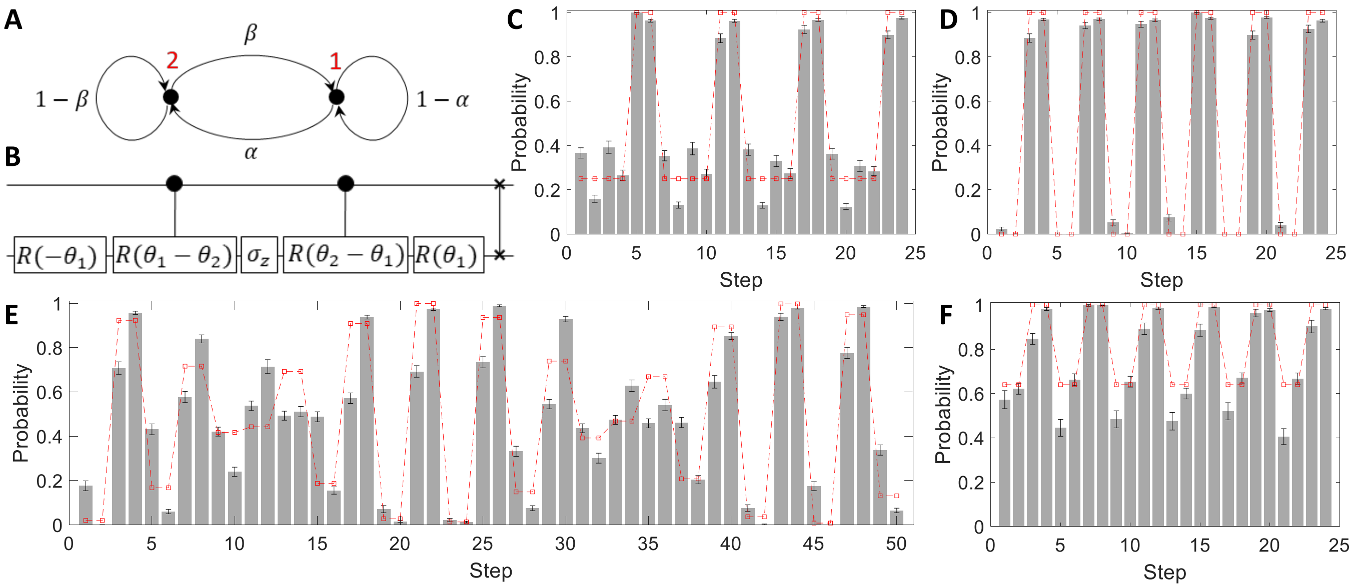

FIG. 4: **Experimental quantum simulation of Szegedy directed quantum walks.** (A) A weighted two-node graph. Edge weights are decided by $\alpha, \beta \in [0,1]$. (B) Quantum circuit for a single-step SQW on the two-node graph. $R(\theta)$ is defined as $R(\theta) = [\cos\theta, -\sin\theta; \sin\theta, \cos\theta]$ with $\theta \in \{\theta_1, -\theta_1, (\theta_1-\theta_2), (\theta_2-\theta_1)\}$ where $\theta_1 = \arccos(\sqrt{1-\alpha})$ and $\theta_2 = \arccos(\sqrt{\beta})$. (C-F) Theoretical (red points) and experimental (gray bars) probability distributions (of the walker being at node 1) of SQWs with the initial state $|00\rangle$: (C) $\alpha = \beta = 0.25$, $F_{\text{avg}} = 98.46 \pm 0.04\%$; (D) $\alpha = \beta = 0.5$, $F_{\text{avg}} = 98.48 \pm 0.04\%$; (E) $\alpha = \beta = 0.43$, $F_{\text{avg}} = 98.02 \pm 0.04\%$; (F) $\alpha = 0.1, \beta = 0.9$, $F_{\text{avg}} = 98.35 \pm 0.15\%$. The s.d. of each individual probability is also plotted, which is calculated by propagating error assuming Poissonian statistics.

set $[0,2\pi]^p \times [0,\pi]^p$—to find the best $\vec{\gamma}$ and $\vec{\beta}$ for maximizing $\langle \vec{\gamma}, \vec{\beta}|C|\vec{\gamma}, \vec{\beta}\rangle$[39]. With p getting increased, the quality of the approximation of QAOA improves[26].

In our experiments, we restricted to the $p = 1$ case of QAOA, and applied QAOA to three 2-bit CSPs. The corresponding quantum circuits are shown in Fig. 3(A). The first CSP (denoted as CSP_1) is the 2-bit Max2Xor problem which has just one constraint as $C(z) = \frac{1}{2} + \frac{1}{2}z_1 z_2$ where $z_1, z_2 \in \{\pm 1\}$. The other two CSPs have three constraints:

$$\text{CSP}_2: \tag{11}$$
$$C_1(z) = \tfrac{1}{2} + \tfrac{1}{2}z_1; C_2(z) = \tfrac{1}{2} + \tfrac{1}{2}z_2; C_3(z) = \tfrac{1}{2} + \tfrac{1}{2}z_1 z_2$$
$$\text{CSP}_3: \tag{12}$$
$$C_1(z) = \tfrac{1}{2} + \tfrac{1}{2}z_1; C_2(z) = \tfrac{1}{2} + \tfrac{1}{2}z_2; C_3(z) = \tfrac{1}{2} - \tfrac{1}{2}z_1 z_2$$

For the $p = 1$ QAOA, there are only two angles, γ and β, to be found for optimizing $\langle \gamma, \beta|C|\gamma, \beta\rangle$. We search γ and β along a fine grid on the compact set $[0, 2\pi] \times [0, \pi]$ and show each obtained value of $\langle \gamma, \beta|C|\gamma, \beta\rangle$ as in Fig. 3(B,C) where the target angles are marked as the reddest block. By measuring the corresponding $|\gamma, \beta\rangle$ state in the computational basis for CSP_1, we obtain "00" or "11" with highest probability, corresponding to the target string of CSP_1: $\{z_1, z_2\} = \{1, 1\}$ or $\{-1, -1\}$. Similarly, the obtained results for CSP_2 is $\{z_1, z_2\} = \{1, 1\}$ and for CSP_3 are $\{z_1, z_2\} = \{1, 1\}$, $\{1, -1\}$ or $\{-1, 1\}$—either of which is a solution of CSP_3. The experimental results are shown in Fig. 3(D), with the classical fidelities between experiment and theory of 99.88±0.10%, 96.98±0.56% and 99.48±0.27% respectively.

4. Simulating Szegedy Quantum Walks. Quantum walks model a quantum particle's random movement in a discretized space according to a given set of rules known as a graph. They are of interest for developing quantum computing (e.g. Ref. 40) and quantum algorithms (e.g. Ref. 41) and as an observable quantum phenomena[11]. The Szegedy quantum walk (SQW)[28,29] is a particular class that allows unitary evolution on directed and weighted graphs—which the standard discrete-time and continuous-time quantum walk formalisms do not permit—and has been proposed for application to quantum speedup for ranking the relative importance of nodes in connected database[42–44]. The realization of SQW-based algorithms on a quantum computer requires an efficient quantum circuit implementation for the walk itself[45,46]. Here we have implemented SQW experimentally on an example two-node graph with four weighted directed edges.

A general weighted graph G with N nodes can be described by its transition matrix P where an element $P_{i,j}$ is given by the weight of a directed edge from node i to j, satisfying $\sum_{i=0}^{N-1} P_{i,j} = 1$. A SQW on G is defined as a discrete-time unitary time evolution on a Hilbert space $H = H_1 \otimes H_2$ where H_1 and H_2 are both N-dimensional Hilbert spaces, and thus its quantum circuit implementation requires $2 \log N$ many qubits. The single-step operator of an SQW is given by $U_{\mathrm{sz}} = S(2\Pi - I)$. Here S is a SWAP operator defined as $S = \sum_{i=0}^{N-1}\sum_{j=0}^{N-1} |i,j\rangle\langle j,i|$, and Π is a projection operator as $\Pi = \sum_{i=0}^{N-1} |\phi_i\rangle\langle\phi_i|$ with $|\phi_i\rangle = |i\rangle \otimes \sum_{j=0}^{N-1}\sqrt{P_{j+1,i+1}}\,|j\rangle$ for $i \in \{0, \cdots, N-1\}$. For the example two-node graph that we label $\mathcal{E}$ and sketched in Fig. 4(A), a quantum circuit implementation for single-step SQW operator can be constructed by using the scheme proposed in ref[46], as shown in Fig. 4(B). Repeating this circuit generates an efficient quantum circuit implementation of multiple-step SQWs, which can easily simulate the dynamics of SQWs on the example graph and its variants.

The periodicity of SQWs is determined by the eigenvalues of the single-step operator U_{sz}, and it has been studied on several families of finite graphs[47]. U_{sz} of the graph $\mathcal{E}$ has four eigenvalues: $\{-1, 1, 1-s-\sqrt{s^2-2s}, 1-s+\sqrt{s^2-2s}\}$ where $s = \alpha+\beta$ and $\alpha, \beta \in [0,1]$. U_{sz} is periodic if and only if there exists an integer n such that $\lambda_i^n = 1$ for all four eigenvalues λ_i of U_{sz}. The period is then given by the lowest common multiple of the periods of the eigenvalues. $\mathcal{E}$ has a symmetric transition matrix when $\alpha = \beta$. For SQWs on a symmetric graph $\mathcal{E}$, periodic walks exist in the cases $\alpha = \beta = \frac{1}{4}, \frac{1}{2}, \frac{3}{4}, 1$—with periods of 6, 4, 6 and 2 steps respectively—of which the first two are experimentally verified as shown in Fig. 4(C) and (D). SQWs on a general instance of $\mathcal{E}$ do not exhibit perfect periodicity, as shown by Fig. 4(E) that shows the behaviour of SQWs on $\mathcal{E}$ with $\alpha = \beta = 0.43$. $\mathcal{E}$ has an asymmetric transition matrix when $\alpha \neq \beta$, and perfect periodicities of SQWs can exist in particular cases, such as $\alpha + \beta = 1$, which has a period of 4 steps. An example of this kind, $\alpha = 0.1, \beta = 0.9$, is shown in Fig. 4(F). In our device, we can also perform state tomography on a given time-evolved state of SQWs — we have performed quantum state tomography for more than 500 time-evolved states, observing an average state fidelity of 93.95±2.52% with theoretical prediction.

5. Discussion. The computational capacity of the linear-combination protocol can be expanded by increasing the dimensionality of each linear-combination term. The high-dimensional quantum state can be easily prepared, manipulated and measured with Reck et al.- style linear optical network[15]. For example, a four-qubit Tofolli gate can be effectively implemented through a four-qubit version of the linear-combination protocol that utilizes a two-photon six-dimensional entanglement and four-dimensional Reck et al.- style circuits, as illustrated in the Supplementary Information. However, the linear-combination protocol has its limitation on scaling up for universal quantum computation, as its success probability is inversely proportional to the number of terms. Although the protocol cannot be targeted for the ultimate quantum computer, it possesses great potential in the near- and mid-term for situations where the photonic components are easier to create than the photons themselves and it is no less demanding of individual component performance than other linear optics approaches to QIP. Our range of demonstrations with a single device has shown that the linear-combination scheme is valuable in permitting QIP demonstrations with the current state of the art in photonics and that silicon photonics is capable of fulfilling its requirements. The device reported comprises nonlinear photon sources, optical filtering and reconfigurable linear optics and it was fabricated with a standard CMOS based silicon photonics processes onto a single photonic chip. It generates photons, encodes quantum information on them, manipulates them and performs tomographic measurement, all with high fidelity quantum control for thousands of configurations. From our experience, our demonstrations of the QAOA and SQWs are beyond the practicality and performance achievable with free-space bulk optical experiments and glass-based integrated photonics. Together with developing multi-photon sources[48] and integration with on chip detection[49], future iterations of silicon photonics opens the way to more sophisticated photonic experiments that are impossible to achieve otherwise, including the eventual full-scale universal quantum technologies using light[50].

Data access statement: The data that support the findings of this study are available from the corresponding author upon reasonable request.

* Electronic address: zhouxq8@mail.sysu.edu.cn
† Electronic address: jonathan.matthews@bristol.ac.uk

1 T. D. Ladd, F. Jelezko, R. Laflamme, Y. Nakamura, C. Monroe, and J. L. O'Brien. Quantum computers. *Nature*, 464:45–53, 2010.

2 J. W. Silverstone, D. Bonneau, J. L. O'Brien, and M. G. Thompson. Silicon quantum photonics. *IEEE Journal of Selected Topics in Quantum Electronics*, 22:390 – 402, 2016.

3 Jeremy L O'Brien, Akira Furusawa, and Jelena Vučković. Photonic quantum technologies. *Nature Photonics*, 3(12):687–695, 2009.

4 Callum M. Wilkes, Xiaogang Qiang, Jianwei Wang, Raffaele Santagati, Stefano Paesani, Xiaoqi Zhou, David A. B. Miller, Graham D. Marshall, Mark G. Thompson, and Jeremy L. O'Brien. 60db high-extinction auto-configured mach–zehnder interferometer. *Optics Letters*, 41:5318–5321, 2016.

5 Jie Sun, Erman Timurdogan, Ami Yaacobi, Ehsan Shah Hosseini, and Michael R Watts. Large-scale nanophotonic phased array. *Nature*, 493(7431):195, 2013.

6 Nicholas C Harris, Gregory R Steinbrecher, Mihika Prabhu, Yoav Lahini, Jacob Mower, Darius Bunandar, Changchen Chen, Franco NC Wong, Tom Baehr-Jones, Michael Hochberg, et al. Quantum transport simulations in a programmable nanophotonic processor. *Nature Pho-*

tonics, 11(7):447, 2017.
[7] Emanuel Knill, Raymond Laflamme, and Gerald J Milburn. A scheme for efficient quantum computation with linear optics. *Nature*, 409(6816):46–52, 2001.
[8] Xiao-Qi Zhou, Timothy C Ralph, Pruet Kalasuwan, Mian Zhang, Alberto Peruzzo, Benjamin P Lanyon, and Jeremy L O'Brien. Adding control to arbitrary unknown quantum operations. *Nature communications*, 2:413, 2011.
[9] Long Gui-Lu. General quantum interference principle and duality computer. *Communications in Theoretical Physics*, 45(5):825, 2006.
[10] Alberto Politi, Martin J Cryan, John G Rarity, Siyuan Yu, and Jeremy L O'Brien. Silica-on-silicon waveguide quantum circuits. *Science*, 320(5876):646–649, 2008.
[11] Alberto Peruzzo, Mirko Lobino, Jonathan CF Matthews, Nobuyuki Matsuda, Alberto Politi, Konstantinos Poulios, Xiao-Qi Zhou, Yoav Lahini, Nur Ismail, Kerstin Wörhoff, et al. Quantum walks of correlated photons. *Science*, 329(5998):1500–1503, 2010.
[12] Justin B Spring, Benjamin J Metcalf, Peter C Humphreys, W Steven Kolthammer, Xian-Min Jin, Marco Barbieri, Animesh Datta, Nicholas Thomas-Peter, Nathan K Langford, Dmytro Kundys, et al. Boson sampling on a photonic chip. *Science*, 339(6121):798–801, 2013.
[13] Max Tillmann, Borivoje Dakić, René Heilmann, Stefan Nolte, Alexander Szameit, and Philip Walther. Experimental boson sampling. *Nature Photonics*, 7(7):540–544, 2013.
[14] Andrea Crespi, Roberto Osellame, Roberta Ramponi, Daniel J Brod, Ernesto F Galvao, Nicolò Spagnolo, Chiara Vitelli, Enrico Maiorino, Paolo Mataloni, and Fabio Sciarrino. Integrated multimode interferometers with arbitrary designs for photonic boson sampling. *Nature Photonics*, 7(7):545–549, 2013.
[15] Jacques Carolan, Christopher Harrold, Chris Sparrow, Enrique Martín-López, Nicholas J Russell, Joshua W Silverstone, Peter J Shadbolt, Nobuyuki Matsuda, Manabu Oguma, Mikitaka Itoh, et al. Universal linear optics. *Science*, 349(6249):711–716, 2015.
[16] Jay E Sharping, Kim Fook Lee, Mark A Foster, Amy C Turner, Bradley S Schmidt, Michal Lipson, Alexander L Gaeta, and Prem Kumar. Generation of correlated photons in nanoscale silicon waveguides. *Optics express*, 14(25):12388–12393, 2006.
[17] F. Najafi, J. Mower, N. Harris, F. Bellie, A. Dane, C. Lee, P. Kharel, F. Marsili, S. Assefa, K. K. Berggren, and D. Englund. On-chip detection of entangled photons by scalable integration of single-photon detectors. *Nature Communications*, 6:5873, 2014.
[18] S. Debnath, N. M. Linke, C. Figgatt, K. A. Landsman, K. Wright, and C. Monroe. Demonstration of a small programmable quantum computer with atomic qubits. *Nature*, 536:63–66, 2016.
[19] Lieven MK Vandersypen, Matthias Steffen, Gregory Breyta, Costantino S Yannoni, Mark H Sherwood, and Isaac L Chuang. Experimental realization of shor's quantum factoring algorithm using nuclear magnetic resonance. *Nature*, 414(6866):883–887, 2001.
[20] C. Song, K. Xu, W. Liu, C. Yang, S.-B. Zheng, H. Deng, Q. Xie, K. Huang, Q. Gou, L. Zhang, P. Zhang, D. Xu, D. Zheng, X. Zhu, H. Wang, Y.-A. Chen, C.-Y. Lu, S. Han, and J.-W. Pan. 10-qubit entanglement and parallel logic operations with a superconducting circuit. *Phys. Rev. Lett*, 119:180511, 2017.
[21] Enrique Martín-López, Anthony Laing, Thomas Lawson, Roberto Alvarez, Xiao-Qi Zhou, and Jeremy L O'Brien. Experimental realization of shor's quantum factoring algorithm using qubit recycling. *Nature Photonics*, 6(11):773–776, 2012.
[22] Stefanie Barz, Ivan Kassal, Martin Ringbauer, Yannick Ole Lipp, Borivoje Dakić, Alán Aspuru-Guzik, and Philip Walther. A two-qubit photonic quantum processor and its application to solving systems of linear equations. *Scientific reports*, 4, 2014.
[23] Jianwei Wang, Stefano Paesani, Raffaele Santagati, Sebastian Knauer, Antonio A Gentile, Nathan Wiebe, Maurangelo Petruzzella, Jeremy L O'Brien, John G Rarity, Anthony Laing, et al. Experimental quantum hamiltonian learning. *Nature Physics*, 13(6):551–555, 2017.
[24] R Santagati, J W Silverstone, M J Strain, M Sorel, S Miki, T Yamashita, M Fujiwara, M Sasaki, H Terai, M G Tanner, C M Natarajan, R H Hadfield, J L O'Brien, and M G Thompson. Silicon photonic processor of two-qubit entangling quantum logic. *Journal of Optics*, 19(11):114006, 2017.
[25] D. Hanneke, J. P. Home, J. D. Jost, J. M. Amini, D. Leibried, and D. J. Windeland. Realization of a programmable two-qubit quantum processor. *Nature Physics*, 6:13–16, 2010.
[26] Edward Farhi, Jeffrey Goldstone, and Sam Gutmann. A quantum approximate optimization algorithm. *arXiv preprint arXiv:1411.4028*, 2014.
[27] Edward Farhi, Jeffrey Goldstone, and Sam Gutmann. A quantum approximate optimization algorithm applied to a bounded occurrence constraint problem. *arXiv preprint arXiv:1412.6062*, 2014.
[28] Mario Szegedy. Spectra of quantized walks and a $\sqrt{\delta\epsilon}$ rule. *arXiv preprint quant-ph/0401053*, 2004.
[29] Mario Szegedy. Quantum speed-up of markov chain based algorithms. In *Foundations of Computer Science, 2004. Proceedings. 45th Annual IEEE Symposium on*, pages 32–41. IEEE, 2004.
[30] Andrew M. Childs and Nathan Wiebe. Hamiltonian simulation using linear combinations of unitary operations. *Quantum Info. Comput.*, 12(11-12):901–924, November 2012.
[31] Andrew M Childs, Robin Kothari, and Rolando D Somma. Quantum algorithm for systems of linear equations with exponentially improved dependence on precision. *SIAM Journal on Computing*, 46(6):1920–1950, 2017.
[32] Raj B Patel, Joseph Ho, Franck Ferreyrol, Timothy C Ralph, and Geoff J Pryde. A quantum fredkin gate. *Science advances*, 2(3):e1501531, 2016.
[33] Shi-Jie Wei, Dong Ruan, and Gui-Lu Long. Duality quantum algorithm efficiently simulates open quantum systems. *Scientific Reports*, 6:30727, 2016.
[34] Xiaogang Qiang, Xiaoqi Zhou, Kanin Aungskunsiri, Hugo Cable, and Jeremy O'Brien. Quantum processing by remote quantum control. *Quantum Science and Technology*, 2(4):045002, 2017.
[35] See further details in the Supplementary Information.
[36] Joshua W Silverstone, Damien Bonneau, Kazuya Ohira, Nob Suzuki, Haruhiko Yoshida, Norio Iizuka, Mizunori Ezaki, Chandra M Natarajan, Michael G Tanner, Robert H Hadfield, et al. On-chip quantum interference between silicon photon-pair sources. *Nature Photonics*, 8(2):104–108, 2014.
[37] Robert Raussendorf and Hans J Briegel. A one-way quan-

tum computer. *Physical Review Letters*, 86(22):5188, 2001.
[38] Ryo Okamoto, Jeremy L O'Brien, Holger F Hofmann, Tomohisa Nagata, Keiji Sasaki, and Shigeki Takeuchi. An entanglement filter. *Science*, 323(5913):483–485, 2009.
[39] Edward Farhi and Aram W Harrow. Quantum supremacy through the quantum approximate optimization algorithm. *arXiv preprint arXiv:1602.07674*, 2016.
[40] Andrew M Childs, David Gosset, and Zak Webb. Universal computation by multiparticle quantum walk. *Science*, 339(6121):791–794, 2013.
[41] Andrew M Childs and Jeffrey Goldstone. Spatial search by quantum walk. *Physical Review A*, 70(2):022314, 2004.
[42] Giuseppe Davide Paparo and MA Martin-Delgado. Google in a quantum network. *Scientific reports*, 4, 2012.
[43] Giuseppe Davide Paparo, Markus Müller, Francesc Comellas, and Miguel Angel Martin-Delgado. Quantum google in a complex network. *Scientific reports*, 3, 2013.
[44] T Loke, JW Tang, J Rodriguez, M Small, and JB Wang. Comparing classical and quantum pageranks. *Quantum Information Processing*, 16(1):25, 2017.
[45] Chen-Fu Chiang, Daniel Nagaj, and Pawel Wocjan. Efficient circuits for quantum walks. *Quantum Information & Computation*, 10(5&6):420–434, 2010.
[46] T Loke and JB Wang. Efficient quantum circuits for szegedy quantum walks. *Annals of Physics*, 382:64–84, 2017.
[47] Yusuke Highchi, Norio Konno, Iwao Sato, and Etsuo Segawa. Periodicity of the discrete-time quantum walk on a finite graph. *Interdisciplinary Information Sciences*, 23(1):75–86, 2017.
[48] Matthew J Collins, Chunle Xiong, Isabella H Rey, Trung D Vo, Jiakun He, Shayan Shahnia, Christopher Reardon, Thomas F Krauss, MJ Steel, Alex S Clark, et al. Integrated spatial multiplexing of heralded single-photon sources. *Nature communications*, 4, 2013.
[49] S. Khasminskaya, F. Pyatkov, K. Slowik, S. Ferrari, O. Kahl, V. Kovalyuk, A. Rath, P. adn Vetter, F. Hennrich, M. M. Kappes, G. Goltsman, A. Korneev, C. Rockstuhl, R. Krupke, and W. H. P. Pernice. Fully integrated qunatum photonic circuit with an electrically driven light source. *Nature Photonics*, 10:727–732, 2016.
[50] M. Gimeno-Segovia, P. J. Shadbolt, D. E. Browne, and T. Ruddolph. From three-photon GHZ states to ballistic universal quatum computation. *PRL*, 115:020502, 2015.